GEOPHYSICS, VOL. 64, NO. 1 (JANUARY-FEBRUARY 1999); P. 48–60, 10 FIGS., 3 TABLES.

Stability analysis and improvement of structural index estimation in Euler deconvolution

Valéria C. F. Barbosa*, João B. C. Silva‡, and Walter E. Medeiros**

ABSTRACT

Euler deconvolution has been widely used in automatic aeromagnetic interpretations because it requires no prior knowledge of the source magnetization direction and assumes no particular interpretation model, provided the structural index defining the anomaly falloff rate related to the nature of the magnetic source, is determined in advance. Estimating the correct structural index and electing optimum criteria for selecting candidate solutions are two fundamental requirements for a successful application of this method.

We present a new criterion for determining the structural index. This criterion is based on the correlation between the total-field anomaly and the estimates of an unknown base level. These estimates are obtained for each position of a moving data window along the observed profile and for several tentative values for the structural index. The tentative value for the structural index producing the smallest correlation is the best estimate of the correct structural index. We also propose a new criterion to select the best solutions from a set of previously computed candidate solutions, each one associated with a particular position of the moving data window. A current criterion is to select only those candidates producing a standard deviation for the vertical position of the source smaller than a threshold value. We propose that in addition to this criterion, only those candidates producing the best fit to the known quantities (combinations of anomaly and its gradients) be selected. The proposed modifications to Euler deconvolution can be implemented easily in an automated algorithm for locating the source position.

The above results are grounded on a theoretical uniqueness and stability analysis, also presented in this paper, for the joint estimation of the source position, the base level, and the structural index in Euler deconvolution. This analysis also reveals that the vertical position and the structural index of the source cannot be estimated simultaneously because they are linearly dependent; the horizontal position and the structural index, on the other hand, are linearly independent. For a known structural index, estimates of both horizontal and vertical positions are unique and stable regardless of the value of the structural index. If this value is not too small, estimates of the base level for the total field are stable as well.

The proposed modifications to Euler deconvolution were tested both on synthetic and real magnetic data. In the case of synthetic data, the proposed criterion always detected the correct structural index and good estimates of the source position were obtained, suggesting the present theoretical analysis may lead to a substantial enhancement in practical applications of Euler deconvolution. In the case of practical data (vertical component anomaly over an iron deposit in the Kursk district, Russia), the estimated structural index (corresponding to a vertical prism) was in accordance with the known geology of the deposit, and the estimates of the depth and horizontal position of the source compared favorably with results reported in the literature.

Manuscript received by the Editor October 28, 1996; revised manuscript received March 2, 1998.
*Formerly Dep. Geofísica, CG, Federal University of Pará; currently LNCC, Av. Getulio Vargas 333, Quitandinha, 25651 070 Petropolis, RJ, Brazil; E-mail: valcris@lncc.br.
‡Formerly Dep. Geofísica, CG, Federal University of Pará; currently LNCC, Av. Getulio Vargas 333, Quitandinha, 25651 070 Petropolis, RJ, Brazil; E-mail: jbatista@lncc.br.
**Dep. Física/CCET, Federal University of Rio Grande do Norte, Caixa Postal 1641, 59.072-970 Natal, RN, Brazil; E-mail: walter@dfte.ufrn.br.
© 1999 Society of Exploration Geophysicists. All rights reserved.

INTRODUCTION

Euler's homogeneity equation has long been used to determine either the depth or the nature of a simple equivalent source (e.g., single pole, point dipole, line of dipoles). Hood (1965) uses the 2-D version of Euler's equation combined with the method of characteristic points to obtain a relationship among the depth z_o, the maximum of the total-field anomaly $\Delta T_{\max}$, the maximum of the vertical gradient $[(\partial \Delta T)/(\partial z_o)]_{\max}$, and the structural index η, which is related to the equivalent source nature. If η is known a priori, z_o may be determined because $\Delta T_{\max}$ and $[(\partial \Delta T)/(\partial z_o)]_{\max}$ are known quantities.

Slack et al. (1967) and Barongo (1984) use the same strategy to determine z_o given η and η given z_o, respectively. To reduce the influence of the particular noise realization on parameter estimates, some authors apply Euler's equation at several observation points and form a system of linear equations to simultaneously determine either z_o and η (Ruddock et al., 1966; Slack et al., 1967) or x_o, z_o, and a base level (Thompson, 1982). The simultaneous estimation of z_o and η by Slack et al. (1967), however, is an ill-posed problem with unstable solutions, as can be attested by inspecting their graphical results. This was confirmed numerically in Loures (1991).

Reid et al.'s (1990) extension to 3-D sources of Thompson's (1982) 2-D method became widely used (Paterson et al., 1991; Beasley and Golden, 1993; Hearst and Morris, 1993; Roest and Pilkington, 1993, for example) and was called Euler deconvolution. However, the potential advantage of using Euler's equation, that is, the advantage of assuming no particular geologic model, relies on the correct estimation of the structural index η, which is critical for a meaningful estimation of the source depth (Hsu et al., 1996). As pointed out by Reid (1995), "The choice of structural index remains a vexed problem because structures are poorly imaged and depths are biased if the wrong index is used for a given structure" and "Work remains to develop a reliable method of estimating structural index."

No author mentioned above addresses, analytically, the problem of uniqueness and stability related to estimating the source horizontal and vertical positions, the structural index, and the anomaly base level using Euler's equation. In addition, Thompson (1982) and Reid et al. (1990) assume as correct the structural index producing the tightest cluster of estimates of x_o and z_o, each pair associated to a different position of a moving data window. Besides not being completely objective, this criterion may lead to wrong choices of η.

This paper has two objectives. The first is to perform a theoretical stability analysis for the estimates of parameters x_o, z_o, η, and b, obtained by using just the total-field anomaly and its gradients via Euler's equation. This analysis shows that x_o is independently determined from all other parameters, but z_o cannot be simultaneously estimated with η. Also, if η is known, z_o can be estimated in a unique and stable way. Finally, if η is different from zero, b is also estimated in a unique and stable way. In the case of finite data windows, estimate $\hat{x}_o$ is biased toward the coordinate of the center of the data window. The second objective of this paper is to determine the correct structural index of a simple equivalent source by a procedure based on the strong correlation between the observed total-field anomaly and the estimates of b when a wrong structural index is assumed. By assigning to η several tentative values and computing the corresponding estimates of b, the best estimate of η is the value producing a minimum correlation between the base-level estimates and the total-field anomaly. This criterion was developed analytically and illustrated in synthetic and real data anomalies always leading, in the case of synthetic anomalies, to the correct estimation of the structural index.

The proposed criterion for selecting the structural index can be incorporated easily into an automated interpretation algorithm without substantial increase in the computational load.

METHODOLOGY

The total-field anomaly $\Delta T(x, y, z)$, produced by a point or line source at (x_o, y_o, z_o), referred to a right-hand Cartesian coordinate system, can be represented by the equation

$$\Delta T(x, y, z) = \frac{K}{\left(\sqrt{(x - x_o)^2 + (y - y_o)^2 + (z - z_o)^2}\right)^{\eta}}, \tag{1}$$

where K is a constant. This total-field anomaly obeys Euler's differential equation. For 2-D sources infinitely long in the y-direction, it has the form (Thompson, 1982)

$$(x - x_o)\frac{\partial}{\partial x}\Delta T(x, z) + (z - z_o)\frac{\partial}{\partial z}\Delta T(x, z) = -\eta \Delta T(x, z), \tag{2}$$

where η is known as the structural index and is related to the nature of the source. For example, $\eta = 3$ corresponds to a point dipole, $\eta = 2$ corresponds to a line of dipoles, and $\eta = 1$ is associated with a thin, dipping prism.

We assume that η is known (a criterion to determine η will be presented later) and that ΔT is measured within an additive constant b (the base level) on plane $z =$ constant. The observed total field is given by

$$h^o \equiv h^o(x, z) = \Delta T(x, z) + b. \tag{3}$$

By combining equations (2) and (3), we obtain

$$x_o \frac{\partial}{\partial x}h^o + z_o \frac{\partial}{\partial z}h^o + \eta b = x\frac{\partial}{\partial x}h^o + z\frac{\partial}{\partial z}h^o + \eta h^o. \tag{4}$$

The gradients may be measured or computed from the total-field anomaly using equivalent source transformations (Emilia, 1973) or wavenumber domain filtering (Gunn, 1975).

We present below a theoretical analysis of equation (4) under the ideal assumption that the anomaly and its gradients are continuous functions of x and z known everywhere on the horizontal observation level. The results obtained under this condition will serve as a guideline to explain the behavior of the estimates of source parameters under practical conditions (using a finite, discrete set of observations). To the authors' knowledge, this analysis has never been performed.

Theoretical analysis of Euler's equation

Analytic solution for the source parameters.—We obtain formal estimates for parameters x_o, z_o, and b by solving the following least-squares normal equation associated with equation (4):

$$\mathbf{G}^T\mathbf{G}\mathbf{p} = \mathbf{G}^T\mathbf{y}, \tag{5}$$

where $\mathbf{p}$ is the vector of unknown parameters

$$\mathbf{p} = \begin{bmatrix} x_o \\ z_o \\ b \end{bmatrix}, \tag{6}$$

$$\mathbf{G}^T\mathbf{G} = \begin{bmatrix} \left\langle \frac{\partial}{\partial x}h^o, \frac{\partial}{\partial x}h^o \right\rangle & \left\langle \frac{\partial}{\partial x}h^o, \frac{\partial}{\partial z}h^o \right\rangle & \eta\left\langle \kappa, \frac{\partial}{\partial x}h^o \right\rangle \\ \left\langle \frac{\partial}{\partial x}h^o, \frac{\partial}{\partial z}h^o \right\rangle & \left\langle \frac{\partial}{\partial z}h^o, \frac{\partial}{\partial z}h^o \right\rangle & \eta\left\langle \kappa, \frac{\partial}{\partial z}h^o \right\rangle \\ \eta\left\langle \kappa, \frac{\partial}{\partial x}h^o \right\rangle & \eta\left\langle \kappa, \frac{\partial}{\partial z}h^o \right\rangle & \eta^2\langle \kappa, \kappa \rangle \end{bmatrix}, \tag{7}$$

and

$$\mathbf{G}^T\mathbf{y} = \begin{bmatrix} \left\langle \frac{\partial}{\partial x}h^o, x\frac{\partial}{\partial x}h^o \right\rangle + z\left\langle \frac{\partial}{\partial x}h^o, \frac{\partial}{\partial z}h^o \right\rangle + \eta\left\langle \frac{\partial}{\partial x}h^o, h^o \right\rangle \\ z\left\langle \frac{\partial}{\partial z}h^o, \frac{\partial}{\partial z}h^o \right\rangle + \left\langle \frac{\partial}{\partial z}h^o, x\frac{\partial}{\partial x}h^o \right\rangle + \eta\left\langle \frac{\partial}{\partial z}h^o, h^o \right\rangle \\ \eta\left\langle \kappa, x\frac{\partial}{\partial x}h^o \right\rangle + \eta z\left\langle \kappa, \frac{\partial}{\partial z}h^o \right\rangle + \eta^2\langle \kappa, h^o \rangle \end{bmatrix} \tag{8}$$

and where $\langle u(x), v(x)\rangle$ is the inner product of $u(x)$ and $v(x)$ in the interval $(-L, L)$, defined by

$$\langle u(x), v(x)\rangle \equiv \int_{-L}^{L} u(x)\cdot v(x)\,dx \tag{9}$$

and

$$\kappa \equiv \kappa(x) = 1, \qquad x \in (-L, L). \tag{10}$$

We show in Appendix A that $\langle(\partial/\partial x)h^o, (\partial/\partial z)h^o\rangle$ and $\langle h^o, (\partial/\partial x)h^o\rangle$ are null for a sufficiently large interval $(-L, L)$. Additionally, $\langle \kappa, (\partial/\partial x)h^o\rangle$ and $\langle \kappa, (\partial/\partial z)h^o\rangle$ are also null for large intervals because the integral of any component of the total-field anomaly (and consequently of any of its derivatives) over the horizontal plane is zero (Bhattacharyya, 1967). Additionally, integrating both sides of equation (4) in the interval $(-L, L)$ and taking the above results into account, we learn that $\langle x, (\partial/\partial x)h^o\rangle$ (and, consequently, $\langle \kappa, x(\partial/\partial x)h^o\rangle$) is also null for large intervals. Matrix $\mathbf{G}^T\mathbf{G}$ is therefore diagonal (under the limit $L \to \infty$), and analytic solutions for x_o, z_o, and b may be formally given by

$$\tilde{x}_o = \lim_{L\to\infty} \frac{\left\langle x\frac{\partial}{\partial x}h^o, \frac{\partial}{\partial x}h^o \right\rangle}{\left\langle \frac{\partial}{\partial x}h^o, \frac{\partial}{\partial x}h^o \right\rangle}, \tag{11}$$

$$\tilde{z}_o = \lim_{L\to\infty} \frac{z\left\langle \frac{\partial}{\partial z}h^o, \frac{\partial}{\partial z}h^o \right\rangle + \left\langle x\frac{\partial}{\partial x}h^o, \frac{\partial}{\partial z}h^o \right\rangle + \eta\left\langle h^o, \frac{\partial}{\partial z}h^o \right\rangle}{\left\langle \frac{\partial}{\partial z}h^o, \frac{\partial}{\partial z}h^o \right\rangle}, \tag{12}$$

and

$$\tilde{b} = \lim_{L\to\infty} \left\{ \frac{1}{\eta}\left(\frac{\left\langle \kappa, x\frac{\partial}{\partial x}h^o \right\rangle + z\left\langle \kappa, \frac{\partial}{\partial z}h^o \right\rangle}{\langle \kappa, \kappa \rangle} \right) + \frac{\langle \kappa, h^o\rangle}{\langle \kappa, \kappa\rangle} \right\}. \tag{13}$$

If η is different from zero, equation (13) may be reduced to

$$\tilde{b} = \lim_{L\to\infty} \frac{\langle \kappa, h^o\rangle}{\langle \kappa, \kappa\rangle} \equiv \bar{h}, \tag{14}$$

where $\bar{h}$ is the average of h^o in the interval $(-L, L)$. On the other hand, if η tends to zero, $\tilde{b}$ is undetermined.

Uniqueness and stability analysis.—Equation (11) shows that $\tilde{x}_o$ is the average of x weighted by $[(\partial/\partial x)h^o]^2$. It also shows that even in the case that $\eta = 0$, and as far as $(\partial/\partial x)h^o$ is not too small, $\tilde{x}_o$ is a unique and stable estimator of x_o because it is independent of η and involves only nonnull definite integrals.

Equation (12) shows that $\tilde{z}_o$ and η are linearly dependent and therefore cannot be determined simultaneously. In addition, if $(\partial/\partial z)h^o$ is not too small, $\tilde{z}_o$ is unique and stable. Moreover, a value of η equal to zero, or very small, causes no instability in $\tilde{z}_o$.

Equation (13) shows that $\tilde{b}$ is undetermined if η is equal to zero and, as long as η is not too close to zero, $\tilde{b}$ is unique and stable even when $(\partial/\partial x)h^o$ and $(\partial/\partial z)h^o$ are very small.

In summary, because all inner products in the numerators of equations (11), (12), and (13) are bounded, $\tilde{x}_o$, $\tilde{z}_o$, and $\tilde{b}$ are unique and stable as long as $(\partial/\partial x)h^o$, $(\partial/\partial z)h^o$, and η are not too small.

The stability analysis of parameter estimates with respect to perturbations in h^o must also take into account that matrix $\mathbf{G}$ is affected by the presence of noise in the observed anomaly or observed gradients. According to the results of this theoretical analysis, $\mathbf{G}^T\mathbf{G}$ is diagonal, so that any small perturbation $\boldsymbol{\delta}$ of $\mathbf{G}^T\mathbf{G}$ will produce a diagonal dominant matrix $\mathbf{G}^T\mathbf{G} + \boldsymbol{\delta}$. From the Gershgorin theorem (Ralston and Rabinowitz, 1978) we have

$$|\lambda - g_{ii}| \le \sum_{\substack{i=1 \\ i\neq k}}^{3} |g_{ik}|, \tag{15}$$

where g_{ik} and λ are, respectively, elements and eigenvalues of $\mathbf{G}^T\mathbf{G}+\delta$. Equation (15) shows that these eigenvalues are close to the diagonal elements because the nondiagonal elements of $\mathbf{G}^T\mathbf{G}+\delta$ are small. On the other hand, g_{ii} is also close to g'_{ii}, a diagonal element of $\mathbf{G}^T\mathbf{G}$, which coincides with the eigenvalue λ' of this matrix. Therefore, $\lambda \approx \lambda'$. That is, if $\mathbf{G}^T\mathbf{G}$ is stable, $\mathbf{G}^T\mathbf{G}+\delta$ remains stable.

Practical implications

The analytical solution presented in the previous section was used as a tool in inferring stability conditions about the parameter estimators. However, it cannot be used in practice to compute estimates. To do so, we must necessarily truncate and discretize the total-field anomaly and its derivatives. Equations (5)–(8) may still be used to compute the estimates, with the inner products now defined as

$$\langle u(x)\cdot v(x)\rangle = \sum_{n=1}^{N} u[x^* + (n-1)\Delta x]v[x^* + (n-1)\Delta x], \tag{16}$$

where N is the number of points in a data window, x^* is the coordinate of the leftmost observation in the data window, and Δx is the data spacing.

We analyze here how the stability of $\tilde{x}_o$, $\tilde{z}_o$, and $\tilde{b}$ is affected by the use of finite, discrete inner products and a moving data window. Matrix $\mathbf{G}^T\mathbf{G}$, in this case, is not diagonal but may be diagonal dominant for L not too small, so we use equations (11), (12), and (13) as an approximation. Synthetic tests in a later section confirm this approximation is good for intervals $(-L, L)$ as small as one-third of the anomaly main portion. The numerical values of the inner products shown in equations (11), (12), and (13) now depend on the size of the interval; however, they remain bounded. Consequently, estimates of x_o and z_o remain stable, independent of the value of η, as long as $(\partial/\partial x)h^o$ and $(\partial/\partial z)h^o$ are not negligible. The instability may occur only when the data window is centered on the anomaly tails. Conversely, the most stable estimates for x_o and z_o occur when the data window contains the highest absolute values of the horizontal and vertical gradients. This is in agreement with the criterion established by Fairhead et al. (1994). Estimates of b, on the other hand, remain stable as long as η is not negligible, regardless of the values of $(\partial/\partial x)h^o$ and $(\partial/\partial z)h^o$.

We also analyze the bias in estimates of x_o and b produced by the use of a finite moving data window. If the data window is centered on one of the anomaly tails, $(\partial/\partial x)h^o$ is nearly constant. The weighted average in equation (11) becomes the arithmetic average of the x-coordinates of the points in the data window. As a result, $\tilde{x}_o$ becomes biased toward this value. Surprisingly, this biased estimate of x_o is stable even for very small values of $(\partial/\partial x)h^o$, as demonstrated later with synthetic examples.

In summary, using finite, discrete inner products does not change, qualitatively, the previous theoretical results on stability of parameter estimates. From now on, we use the carat symbol ˆ instead of a tilde ˜ to distinguish estimates computed with a finite data window.

Solution acceptance criterion

Thompson (1982) proposes acceptance of solutions satisfying the inequality

$$\frac{\hat{z}_o}{\eta\sigma_{z_o}} > \epsilon, \tag{17}$$

where ϵ is a user-provided positive scalar, $\hat{z}_o$ is the estimate of z_o, and σ_{z_o} is the standard deviation of $\hat{z}_o$. Thompson (1982) states that for high-resolution data, a reasonable value for ϵ is 20. We show in a later section that the smallest singular value of matrix $\mathbf{G}$ increases with the amplitude of h^o; consequently, σ_{z_o} decreases at these points so that criterion (17) selects solutions associated to data windows close to the anomaly peak.

We propose that, in addition to the above criterion, only the solutions satisfying the inequality

$$\left(\frac{\|\mathbf{y}-\mathbf{G}\hat{\mathbf{p}}\|^2}{N-3}\right)^{1/2} < \gamma \tag{18}$$

be accepted. The positive scalar γ cannot be related directly to the standard deviation of the noise in data because the elements of matrix $\mathbf{G}$ are realizations of a random variable and also because the elements of $\mathbf{y}$ are not total-field observations. Because we look for estimates $\hat{\mathbf{p}}$ satisfying equation

$$\mathbf{G}\mathbf{p} = \mathbf{y} \tag{19}$$

in a quasi-exact way, we set the scalar γ to the smallest positive number still producing coherent solutions.

Selecting the structural index

As pointed out, computing $\hat{\mathbf{p}}$ requires the a priori knowledge of the structural index η. In fact, the choice of a correct structural index has been the main difficulty in applying Euler's deconvolution (Reid, 1995; Hsu et al., 1996). Thompson (1982) and Reid et al. (1990) assume, as correct, the index producing the smallest solution dispersion. We found, however (and show in a later section), that this criterion sometimes may be ambiguous. We derive below, from Euler's equation, a new objective criterion for determining the structural index.

Assume that $z=0$, that estimates $\hat{x}_o$, $\hat{z}_o$, and $\hat{b}$ are associated with the correct structural index η, and that $\hat{x}_{o_i}$, $\hat{z}_{o_i}$, and $\hat{b}_i$ are solutions of equation (4) in the least-squares sense using the observations inside a given moving data window stationed at its ith position. Then we may write

$$\hat{x}_{o_i}\frac{\partial}{\partial x}h^o(x_j) + \hat{z}_{o_i}\frac{\partial}{\partial z}h^o(x_j) + \eta\hat{b}_i = x_j\frac{\partial}{\partial x}h^o(x_j) + \eta h^o(x_j) + \alpha_{ij}, \qquad i = 1, 2, \ldots, M, \tag{20}$$

where $h^o(x_j)$, $(\partial/\partial x)h^o(x_j)$, and $(\partial/\partial z)h^o(x_j)$ are, respectively, the total-field anomaly and its gradients evaluated at any point $x = x_j$ inside the data window, α_{ij} is a residual, and M is the number of positions occupied by the moving data window. Assume also that, using a wrong structural index μ, we obtained

estimates $\hat{x}'_{o_i}$, $\hat{z}'_{o_i}$, and $\hat{b}'_i$ as least-squares solution of equation (4). Then we may write after a minor rearrangement

$$\hat{x}'_{o_i}\frac{\partial}{\partial x}h^o(x_j)+\hat{z}'_{o_i}\frac{\partial}{\partial z}h^o(x_j)+\mu\hat{b}'_i = x_j\frac{\partial}{\partial x}h^o(x_j) + \eta h^o(x_j)+(\mu-\eta)h^o(x_j)+\beta_{ij}, \qquad i=1,\ldots,M, \tag{21}$$

where β_{ij} is a residual. Subtracting equation (20) from equation (21), we get

$$\left(\hat{x}'_{o_i}-\hat{x}_{o_i}\right)\frac{\partial}{\partial x}h^o(x_j)+\left(\hat{z}'_{o_i}-\hat{z}_{o_i}\right)\frac{\partial}{\partial z}h^o(x_j)+\mu\hat{b}'_i-\eta\hat{b}_i = (\mu-\eta)h^o(x_j)+\beta_{ij}-\alpha_{ij}, \qquad i=1,2,\ldots,M \tag{22}$$

or

$$\hat{b}'_i=\frac{\eta}{\mu}\hat{b}_i+\frac{\hat{x}_{o_i}-\hat{x}'_{o_i}}{\mu}\frac{\partial}{\partial x}h^o(x_j)+\frac{\hat{z}_{o_i}-\hat{z}'_{o_i}}{\mu}\frac{\partial}{\partial z}h^o(x_j) + \frac{(\mu-\eta)}{\mu}h^o(x_j)+\frac{\beta_{ij}-\alpha_{ij}}{\eta}, \qquad i=1,2,\ldots,M. \tag{23}$$

Equation (23) shows that the estimate $\hat{b}'_i$ as a function of the data window position may be correlated with the total-field anomaly. This correlation is positive for a tentative structural index greater than the correct one ($\mu > \eta$) and vice versa. The correct index produces a null correlation between the total-field anomaly and the estimate of its base level because the latter will be constant. However, equation (23) shows that the terms containing the horizontal and vertical gradients and the residuals α_{ij} and β_{ij} may interfere in the correlation between $\hat{b}'$ and h^o. To show that the interference of the terms containing the gradients is minimal, recall that the estimate of x_o is independent of the structural index [equation (11)]. So, we may expect that $\hat{x}'_{o_i}\approx\hat{x}_{o_i}$ and the term in equation (23) containing the horizontal gradient does not substantially affect the correlation between h_o and $\hat{b}'$. Similarly, despite the dependence of z_o on η, the vertical gradient has no qualitative effect on this correlation because there is no phase change between the total-field anomaly and its vertical gradient. Equation (12) shows that the estimate of z_o increases with the structural index, so terms $(\hat{z}_{o_i}-\hat{z}'_{o_i})/\mu$ and $(\mu-\eta)/\mu$ in equation (23) are of opposite signs. Depending on which term dominates, either positive or negative correlation of $\hat{b}'$ and h^o may be produced by a structural index greater than the correct one. However, only by chance and in particular cases will the terms involved in the opposite correlations cancel each other. So, the criterion of minimum correlation associated with the correct structural index remains valid. The influence of term $(\beta_{ij}-\alpha_{ij})/\eta$ cannot be predicted easily. We found, heuristically, that the destructive effect of this term (if any) on the correlation between $\hat{b}'$ and h^o is minimized by picking x_j as the position of the data window center.

The practical procedure to determine η is as follows. First, we select the profile interval where the total-field anomaly presents a large horizontal gradient (this makes any correlation with the total-field anomaly more stable and significant). A criterion for selecting automatically this interval is presented in next section. Next, for each tentative index μ, we compute $\hat{\mathbf{p}}$ by solving equation (5) using a finite and discrete inner product at M positions of the moving data window. Then, we define two M-dimensional vectors: the first one is $\mathbf{b}^\mu$, whose kth element is the estimated base level $\hat{b}^\mu_k$ for the kth position of the data window with the tentative index μ; the second vector is $\mathbf{h^o}$, whose kth element is the observed total-field anomaly coinciding with the central point of the data window at its kth moving position. Finally, we compute the correlation coefficient r^μ between $\mathbf{b}^\mu$ and $\mathbf{h^o}$ for each tentative value of μ by the standard discrete correlation formula (Davis, 1973). The estimated structural index $\hat{\eta}$ is the value of μ producing the smallest $|r^\mu|$.

Rigorously, the use of a moving data window is not necessary to obtain the best estimates because the best data intervals (where the gradients are large) can be determined independently from the solutions themselves. Using a moving data window, however, allows the transformation of the ill-posed problem of simultaneously estimating z_o and η into a well-posed problem by introducing additional, independent information about the parameters (namely, the minimum correlation between $\tilde{b}$ and h^o).

TESTS WITH SYNTHETIC DATA

In the following tests, our methodology is applied to synthetic anomalies produced by a horizontal cylinder ($\eta=2$) and by two juxtaposed prisms, simulating a geologic contact ($\eta=0$). The data profile has 100 points in the interval $x\in[1\,\text{km}, 100\,\text{km}]$ for the case of a cylinder and 61 points in the interval $x\in[20\,\text{km}, 80\,\text{km}]$ points for the geologic contact. In both cases, the observations are separated by a 1-km interval and symmetrically distributed about the anomalous source. The moving data window has 7 points. To simulate experimental errors, the data were corrupted with pseudorandom Gaussian noise having zero mean and standard deviation of 2 nT in the case of the horizontal cylinder and 5 nT in the case of the geologic contact. The horizontal and vertical gradients were obtained from the total-field anomaly using equivalent source transformations (Emilia, 1973).

Horizontal cylinder: Structural index 2

Figure 1 shows the total-field anomaly and the horizontal and vertical gradients produced by a horizontal cylinder with a radius of 1 km and the center located at $x_o=50$ km and $z_o=3$ km. For simplicity, the magnetization and the ambient field were assumed to be vertical. However, as pointed out by Reid et al. (1990), this does not restrict application of the method. The magnetization intensity is 3 A/m.

In applying Euler's deconvolution to the data of Figure 1, we considered five possible structural indices μ: 0.5, 1, 1.5, 2, and 3. To demonstrate that matrix $\mathbf{G}^T\mathbf{G}$ is well conditioned even when using a small data window, we show in Figure 2 the smallest singular value s of $\mathbf{G}$ for each possible structural index (μ) against the center of the moving data window. The greater the structural index, the greater is s, as expected. For a fixed μ, s roughly increases with the total-field anomaly. Note that even in the worst case ($\mu=0.5$), s is always greater than 0.3.

Figure 3 shows the estimate $\hat{x}_o$ against the center of the moving window for the correct index $\eta = 2$. In the intervals where the anomaly is almost constant [(0 km, 43 km) and (58 km, 100 km)], $\hat{x}_o$ is biased toward the average of the x-coordinates of the points defining the data window, as already demonstrated analytically [see equation (11)]. This bias, rather than parameter instability, is the main factor producing a striking dispersion of $\hat{x}_o$ when the data window is centered near the anomaly tail. As expected from the analysis of equation (11), this characteristic does not depend on the tentative structural index. This bias forms the basis for an automatic interpretation algorithm using the proposed modifications to Euler deconvolution. First, we obtain vectors $\hat{\mathbf{x}}_\mathbf{o}$ and $\hat{\mathbf{x}}_\mathbf{w}$ whose elements are, respectively, estimates of x_o and the corresponding positions of the data window. Considering $\hat{\mathbf{x}}_\mathbf{o}$ as a function of $\hat{\mathbf{x}}_\mathbf{w}$ as in Figure 3, we fit, in the least-squares sense and in a piecewise fashion, straight lines to $2K + 1$ elements of $\hat{\mathbf{x}}_\mathbf{o}$ lying between $\hat{x}_{o_{i-K}}$ and $\hat{x}_{o_{i+K}}$ for $i = K+1, K+2, \ldots, M-K$, where subscript i stands for the ith position of the center of the data window and M is the number of data window positions along the profile. Integer K should be typically two or three, but it may depend on the size of the data spacing relative to the anomaly width. Then we obtain the slope θ_i of the fitted line with respect to the axis associated with the elements of $\hat{\mathbf{x}}_\mathbf{w}$. The ith position of the center of the data window is then considered to be inside or outside a region containing a magnetic anomaly, depending, respectively, on whether θ_i is close to zero (say, within a few degrees) or not. The segments of the observed profile marked as pertaining to anomalous regions are used in the computation of the correlation between the estimate of the base level and the total-field anomaly to determine the structural index of each individually detected source. Note that determining the intervals pertaining to the anomalous regions, computing the correlation coefficient r^μ, and verifying inequality (18) is the only additional computational load introduced by the proposed modifications to Euler deconvolution relative to the standard application of the method. They involve only simple formula evaluations and do not represent a substantial increase in processing time.

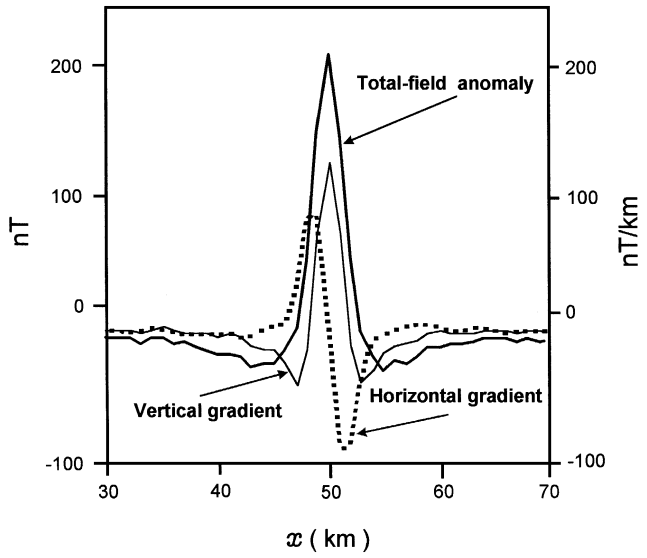

FIG. 1. Total-field anomaly and its vertical and horizontal gradients produced by a horizontal cylinder uniformly magnetized in the vertical direction with a magnetization of 3.0 A/m and whose center is located at $x = 50$ km and $z = 3$ km. The ambient field is vertical.

Figure 4a shows, for all tentative indices, the solutions obtained using criterion (17), and Figure 4b displays the solutions obtained with the proposed criterion [combination of inequalities (17) and (18)] with $\gamma = 15$ nT. Note that condition (18) efficiently contributed to reducing the spray of solutions. By using only criterion (17) and the analysis of solution clustering to select the structural index (Thompson, 1982; Reid et al., 1990), structural indices 1, 1.5, and 2 might be equally accepted, producing rather discrepant estimates of the source depth: 1.75 km, 2.50 km, and 3.1 km, respectively.

To determine the structural index by the proposed criterion, we computed the correlation coefficient r^μ, defined in the interval between $x = 48$ km and $x = 52$ km (selected according to the procedure described above) for each tentative structural index. The results are displayed in Table 1, indicating that the correct index is 2. Graphically, this minimum correlation is illustrated in Figure 5, where the estimated base level is plotted against the center of the moving data window for each tentative structural index. After selecting the (correct) structural index, we note in Figure 4b that the solution corresponding to $\eta = 2$ provides an excellent estimate of the cylinder center.

We stress that the proposed criterion for solution acceptance reduced the possible solutions associated with the correct index ($\eta = 2$) from seven in Figure 4a to just one in Figure 4b. Not accidentaly, the solution for $\eta = 2$ retained in Figure 4b (among the seven possible solutions shown in Figure 4a) was the one closest to the cylinder center. This occurs because the estimation of the position parameters is a stable problem, so that the best-fit criterion [equation (18)] leads to solutions close to the true one as long as the correct structural index is used. A usual best fit criterion in geophysical interpretation does not lead to solutions close to the true one because the geophysical inverse problem is, in general, unstable.

Geologic contact: The structural index zero

Figure 6 displays the total-field anomaly and the horizontal and vertical gradients produced by a simulated geologic contact at $x = 50$ km, consisting of two juxtaposed prisms with semi-infinite thicknesses and widths with top at 2 km below the surface. The prisms have a magnetization contrast of 0.5 A/m and are vertically magnetized.

Before applying the proposed methodology to the data in Figure 6, we make some theoretical and numerical considerations about the case of a zero structural index. Equation (13) shows that, in the case of a zero structural index, the base level b is undetermined. To obtain, in this case, still meaningful

Table 1. Tentative structural index (μ) and the correlation coefficient (r^μ) between $\hat{\mathbf{b}}$ and $\mathbf{h}^\mathbf{o}$ for a horizontal cylinder.

Structural index (μ)	Correlation coefficient (r^μ)
0.5	−0.980
1.0	−0.971
1.5	−0.930
2.0	−0.006
3.0	0.994

estimates of x_o and z_o, Reid et al. (1995) used a modified Euler's equation by effectively eliminating the base level as a parameter and introducing another constant involving the magnetization contrast, the field direction, and strike and dip factors. Alternatively, we use the original equation (4) and avoid indetermination by using values close to zero for the structural index. In practice, the value used for the structural index should be sufficiently small to allow a good representation of the geological model but great enough to retain the effectiveness of criterion (17). The value 0.1 is a good trade-off between these two conflicting requirements.

The indetermination of estimate $\hat{b}$ is confirmed numerically by the large projection of $\hat{b}$ onto the eigenvector associated with the smallest singular value of $\mathbf{G}$. As expected, the stability of $\hat{b}$ decreases as the structural index approaches zero. By using a structural index as small as 10^{-5}, we found that this increasing instability does not invalidate the proposed criterion to determine the structural index (not shown) and does not intefere with the stability of $\hat{x}_o$ and $\hat{z}_o$, as shown by the small projections of these estimates onto the eigenvector associated with the smallest singular value $s_{\min}$ of $\mathbf{G}$ (Figures 7a and b).

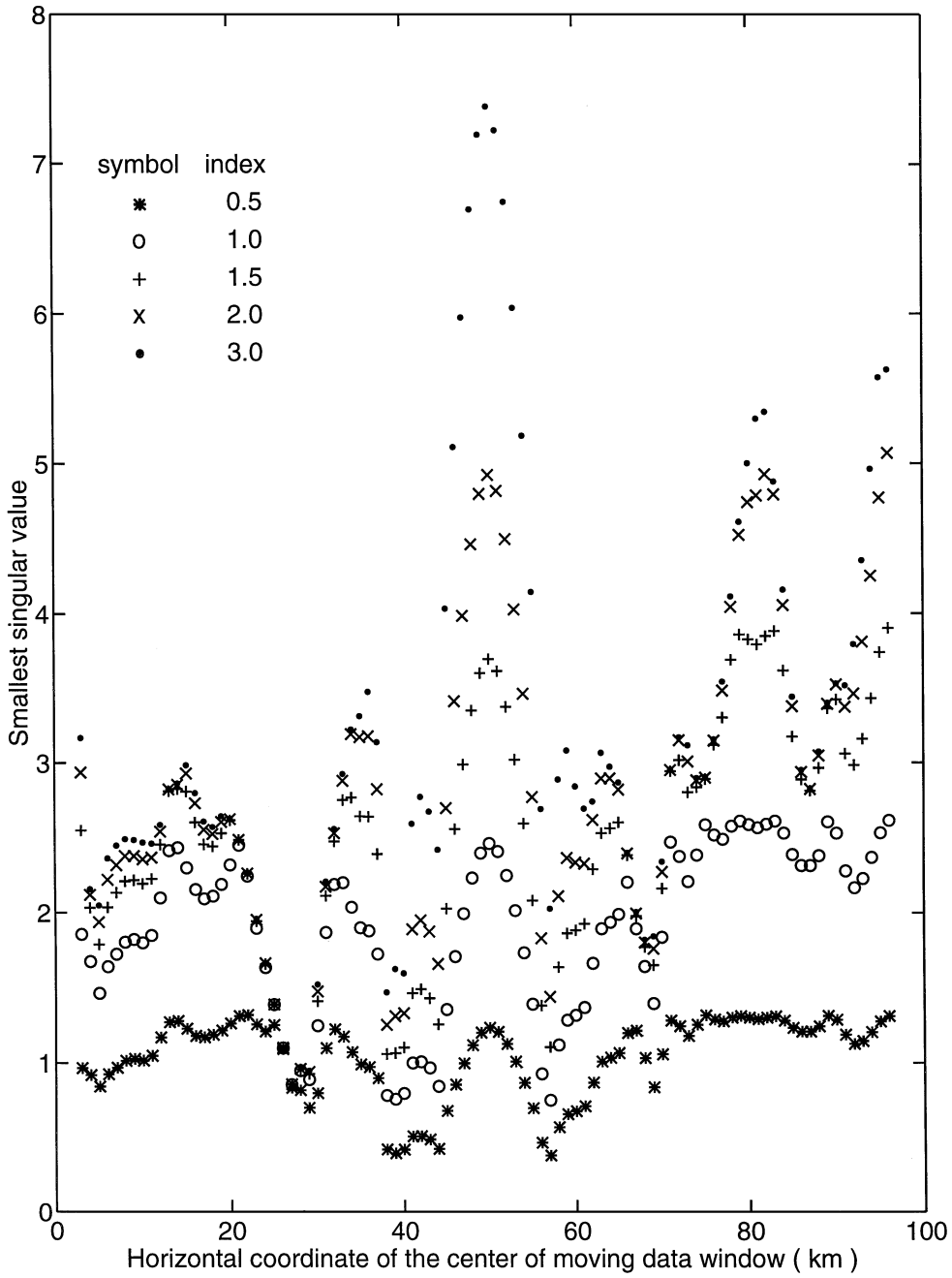

FIG. 2. Smallest singular value of matrix $\mathbf{G}$ against the coordinate of the center of the moving data window for each tentative structural index for the case of a horizontal cylinder. The singular values increase with the structural index. Even for the smallest tentative index (0.5), it is always greater than 0.3, confirming that estimates $\hat{x}_o$, $\hat{z}_o$, and $\hat{b}$ are stable.

Table 2 shows the correlation coefficient r^μ, computed in the interval [24 km, 77 km] of the profile shown in Figure 6, for the possible tentative structural indices 0.1, 1, 1.5, 2, and 3. The minimum of $|r^\mu|$ occurs at $\mu = 0.1$, confirming the validity of the proposed criterion. The inversion results using $\mu = 0.1$ and the proposed criterion of solution acceptance with $\gamma =$ 10 nT produced a set of five acceptable solutions, all lying at the vertical contact ($\hat{x}_o = 50$ km). One solution is 2 km deep, and the others are clustered along the interval $\hat{z}_o = 2.25$ km and $\hat{z}_o = 2.42$ km.

REAL DATA EXAMPLE

Figure 8 shows 20 observations of the vertical component over an iron deposit in the Kursk district in Russia (Werner, 1953). The horizontal and vertical gradients are also shown in the figure and were obtained by the equivalent source technique. A seven-point data window was used; the possible tentative structural indices were 0.5, 1, 1.5, 2, and 3. The inversion results using the proposed criterion with $\gamma = 7000$ nT are shown in Figure 9. To determine the structural index, the correlation coefficient r^μ was computed for each tentative index μ. Table 3 shows that the smallest $|r^\mu|$ occurs at $\mu = 1$, indicating that the

Table 2. Tentative structural index (μ) and the correlation coefficient (r^μ) between $\hat{b}$ and h^o for a geologic contact.

Structural index (μ)	Correlation coefficient (r^μ)
0.1	0.604
1.0	0.948
1.5	0.961
2.0	0.967
3.0	0.972

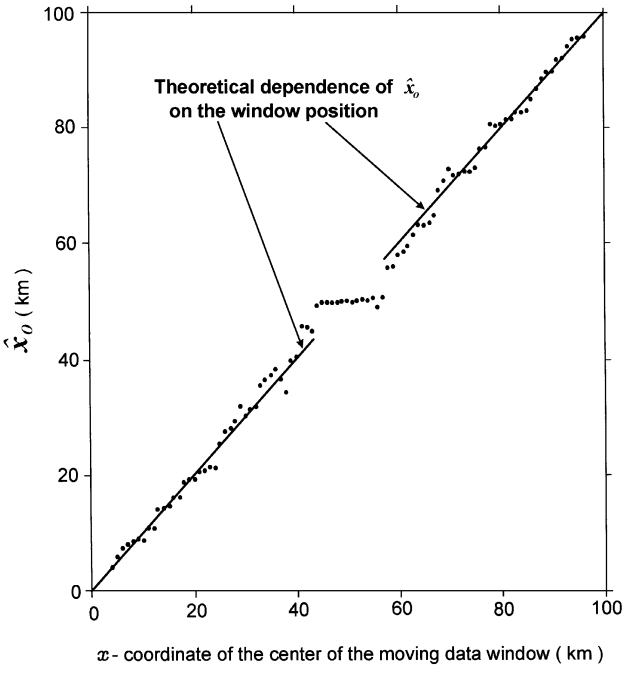

FIG. 3. Horizontal cylinder. Estimates $\hat{x}_o$ (dots) against the coordinate of the center of the moving data window. The figure shows that a correct estimate for x_o is only obtained for data windows containing significant anomaly signal (between $x = 44$ and $x = 57$). Outside this region, $\hat{x}_o$ is a linear function of the window location and not of the position of the actual source. The straight lines show the theoretical dependence of $\hat{x}_o$ on the window position for the case that $(\partial/\partial x)h^o$ is virtually zero. Note that $\hat{x}_o$ is stable even when $(\partial/\partial x)h^o$ is very small (left and right extremes of profile).

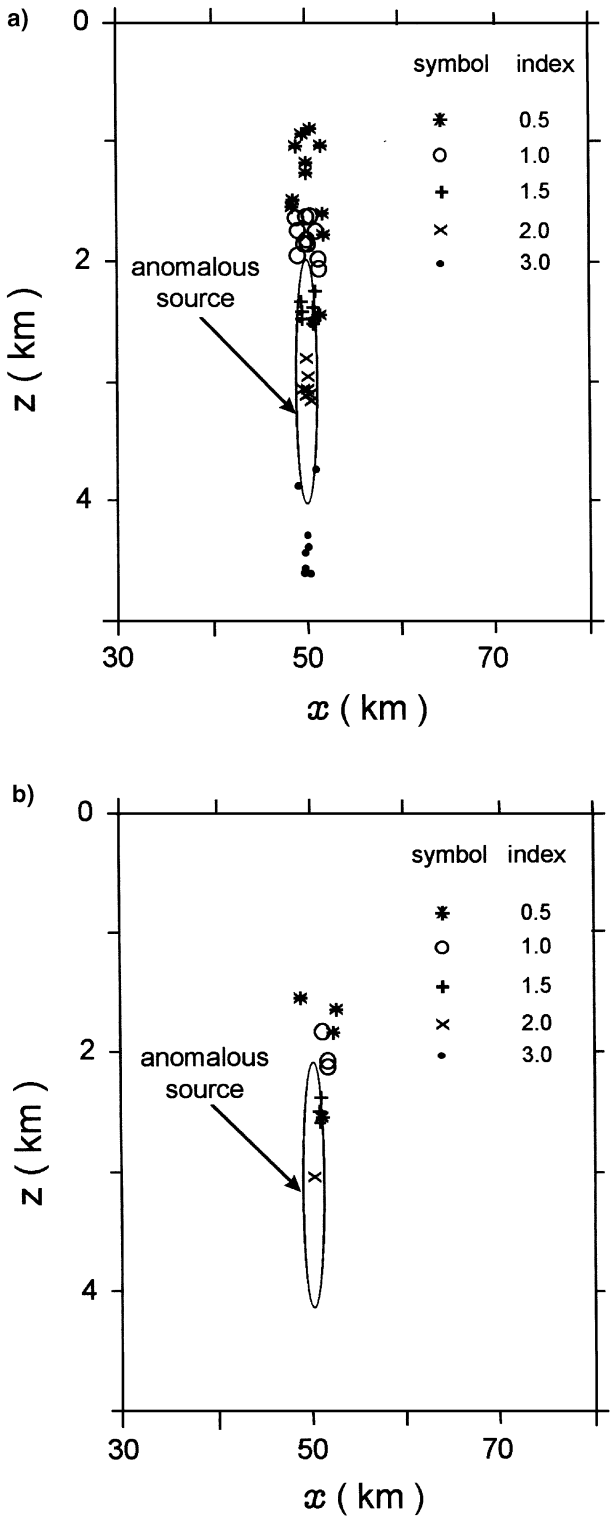

FIG. 4. Horizontal cylinder. Estimates of the source position (a) using Thompson's (1982) criterion [condition (17)]; (b) using the proposed criterion, i.e., combining Thompson's criterion and the best-fit criterion [conditions (17) and (18)] for each tentative structural index. The proposed criterion drastically reduced the number of alternative solutions. For the correct structural index ($\eta = 2$), just one solution is accepted.

Table 3. Tentative structural index (μ) and the correlation coefficient (r^{μ}) between $\hat{b}$ and h^{o} for the Kursk anomaly, Russia.

Structural index (μ)	Correlation coefficient (r^{μ})
0.5	−0.878
1.0	0.161
1.5	0.844
2.0	0.910
3.0	0.935

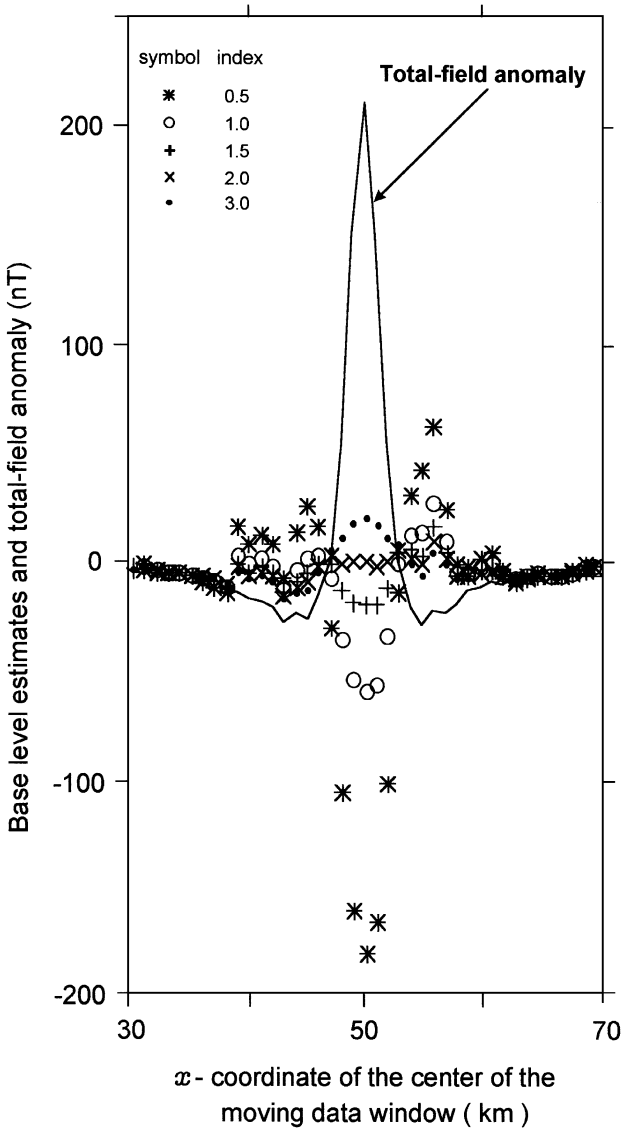

FIG. 5. Horizontal cylinder. Total-field anomaly and estimates $\hat{b}$ against the x-coordinate of the center of the moving data window for each tentative structural index. The figure shows graphically that the assumption of the correct value for the structural index leads to a minimum correlation between the estimates of the base level ($\times$) and the total field anomaly. Base-level estimates obtained by assuming a structural index smaller than the true one produce negative correlations with the observed field ($*$, $\circ$, $+$), while an index greater than the true one produces a positive correlation (dots).

observed anomaly is similar to the anomaly produced by a thin prism. The estimated x-coordinates of the source are in the interval [−4.6 m, −3.1 m], with an average of −3.7 m, and the estimated z-coordinates are in the interval [267.6 m, 269.7 m], with an average of 268.9 m.

Werner (1953) applies to this anomaly the following estimators for the coordinates of the top of a thin prism:

$$\hat{x}_o = \frac{x_1 X_1 - x_2 X_2}{X_1 - X_2} \tag{24}$$

and

$$\hat{z}_o = \frac{-(x_1 - x_2) Z_1}{X_1 - X_2}, \tag{25}$$

where (X_1, Z_1) and (X_2, Z_1) are, respectively, pairs of measurements of the horizontal and vertical components at points x_1 and x_2 where $Z_1 = Z_2$. Both components are shown in Figure 10.

To apply Werner's method, two points x_1 and x_2 are selected where the values of the vertical component are equal. Then, X_1 and X_2 are graphically obtained at these points. If a small value is selected for the Z-component (say, 0.05×10^5 nT), the coordinates x_1 and x_2 will be unstable with respect to errors in the interpolated values of Z. On the other hand, selecting a large value for the Z-component (say, 1.25×10^5 nT) leads to unstable determination of X_1 and X_2 with respect to errors in the interpolated values of Z. In both cases, the estimates of the source coordinates x_o and z_o may contain substantial errors, as may be inferred from equations (24) and (25).

Werner (1953) selected seven pairs of points where the vertical component are equal. The values of Z_1 are 1.25×10^5 nT, 1.0×10^5 nT, 0.75×10^5 nT, 0.50×10^5 nT, 0.25×10^5 nT, 0.15×10^5 nT, and 0.005×10^5 nT. The first two values are close to the anomaly maximum, while the last two are close to the anomaly tail; so it is expected that all these four values produce unstable estimates of x_o and z_o. Werner (1953), however, considered the first four values as producing the best estimates of the source coordinates, and took the averages of them as the best estimates, leading to the averages $\bar{x}_o = -12.6$ m and $\bar{z}_o = 282.0$ m. On the other hand, if we take the average of the estimates that we consider the most stable (associated with a Z-component equal to 0.75×10^5 nT, 0.50×10^5 nT, and 0.25×10^5 nT), we obtain as the average coordinates $\bar{x}_o = 4.2$ m and $\bar{z}_o = 268.9$ m, denoting a much closer agreement with our estimates.

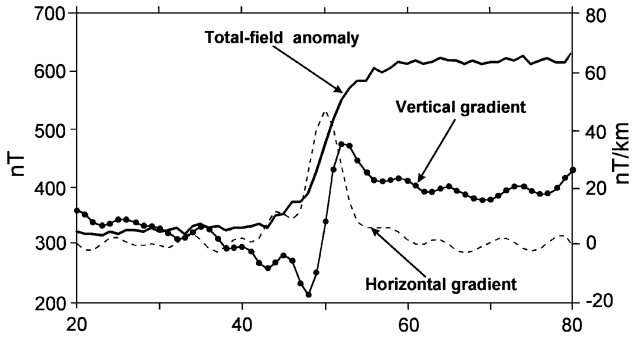

FIG. 6. Total-field anomaly and its vertical and horizontal gradients produced by a vertical contrast located at $x = 50$ km and $z \in [2\text{ km}, \infty]$. The magnetization contrast is 0.5 A/m. The magnetization vector and the ambient field are vertical.

CONCLUSIONS

We present a theoretical analysis of the problem of estimating the source position, the base level, and the structural index in Euler deconvolution. We showed that the horizontal location is correctly estimated despite the assumption of an incorrect structural index, while the vertical location is not. The estimates of the source coordinates using Euler's equation are stable regardless of the tentatively assumed structural indices as long as the data window is not centered at the anomaly tails. For structural indices approaching zero, the base level estimate presents decreasing stability and is undetermined for the zero structural index case. In this case, a practical approach still producing satisfactory estimates of the source position is to approximate the zero structural index by 0.1. To the authors' knowledge, this analysis has never been done before.

We also showed that the cause of the undesirable spray of the solutions in Euler deconvolution is a strong bias of the estimate of the source horizontal position toward the x-coordinate of the center of the data window when the latter is centered on the anomaly tail.

We complemented the criterion of solution acceptance of Thompson (1982) by accepting only the solutions producing the best fit to the known quantities. This additional criterion proved to be effective in reducing the spray of solutions obtained with different positions of the data window.

We also presented a new criterion to determine the structural index based on the correlation of the observed anomaly

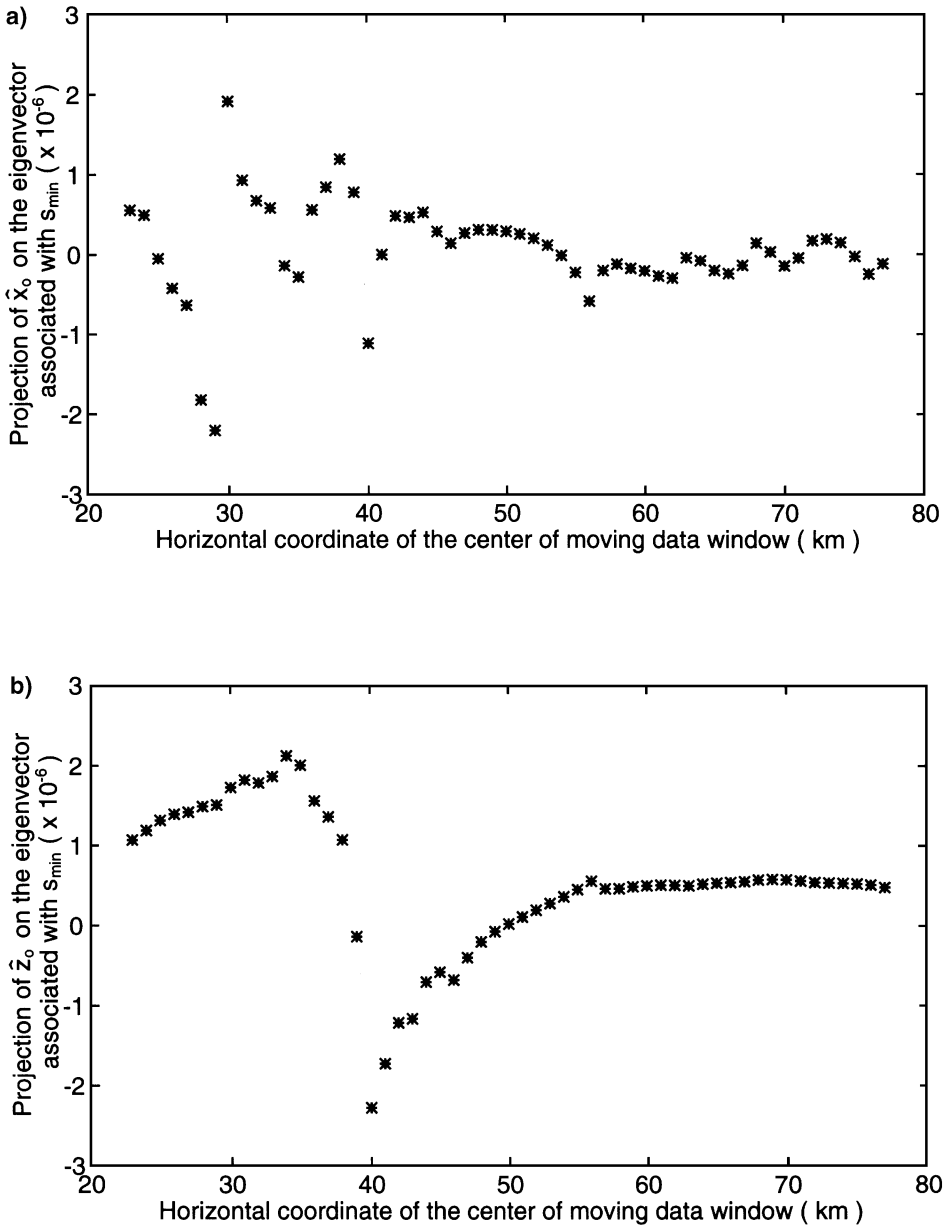

FIG. 7. Vertical contact. Projection of estimates (a) $\hat{x}_o$ and (b) $\hat{z}_o$ on the eigenvector associated with the smallest singular value of $\mathbf{G}$ (computed with $\eta = 10^{-5}$) against the horizontal coordinate of the center of the moving data window. In both cases, the projections are very small, indicating that x_o and z_o do not belong to the null space of $\mathbf{G}$ arisen by the assumption of a small η.

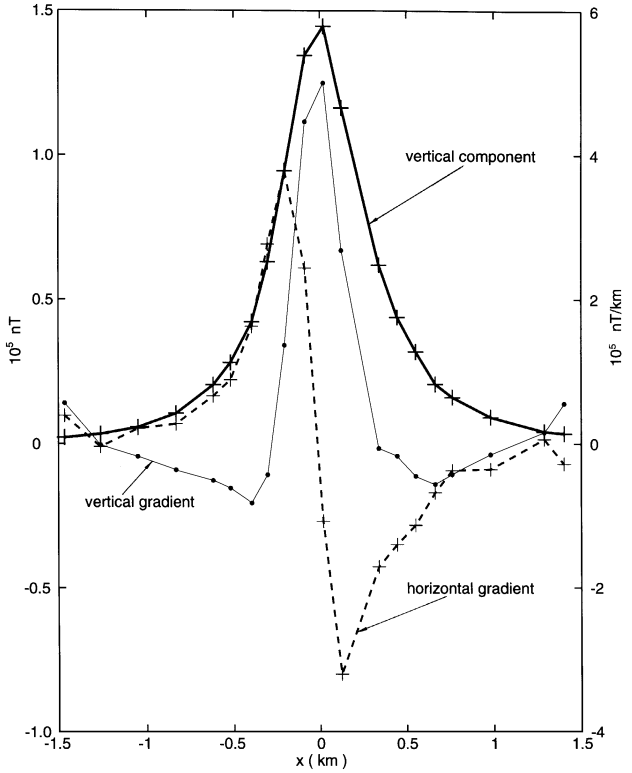

FIG. 8. Vertical component and its vertical and horizontal gradients over an iron deposit at Kursk district, Russia. Thick crosses mark the observations of the vertical component. Thin crosses and dots mark, respectively, the horizontal and vertical gradient values, computed by equivalent source transformation.

with the estimated base level. This criterion, based on the correlation between the estimate of the base level and the observed field, was deduced theoretically from Euler's equation itself and was extensively tested with synthetic data, always producing correct estimates of the structural index. This criterion works even when a tentative structural index is very small, despite the instability of the base-level estimates in this case. Finally, the proposed criterion does not depend on the estimated solutions, which represents an advantage over the criterion of Thompson (1982) and Reid et al. (1990). As a result, a large number of redundant solutions are not needed and, consequently, Euler deconvolution incorporating the proposed modifications may be applied succesfully not only to aeromagnetic surveys but also to ground magnetic surveys having just a few observed data. Both criteria developed in this paper represent, therefore, a substantial improvement in magnetic source mapping using Euler deconvolution.

The proposed modifications to Euler deconvolution can be implemented easily in an automated algorithm for locating the source position. The only additional calculation involves determining the data intervals along which the correlation between the estimated base level and the observed field is computed. These calculations are not computer intensive because they involve only straightforward evaluations of standard data-fitting and correlation formulae. In summary, with a negligible increase in processing time, the proposed modificatons of Euler deconvolution allow the interpreter to produce more reliable estimates of the source position.

The proposed methodology was applied to the vertical field anomaly over an iron deposit at Kursk, Russia. The estimated structural index is one, corresponding to a prism, which is in

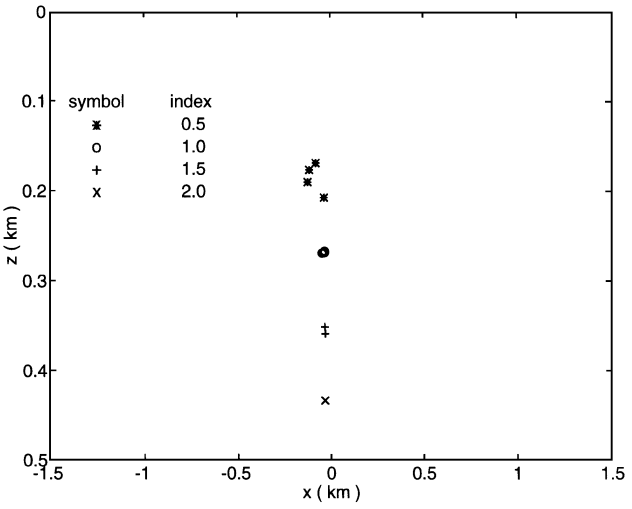

FIG. 9. Kursk anomaly. Source position estimates for each tentative structural index. The estimated index is 1.0, as inferred from the minimum correlation criterion (Table 3). Index $\eta = 1$ implies that the anomalous source has a prismatic shape. The open circles in the figure pinpoint the prism top.

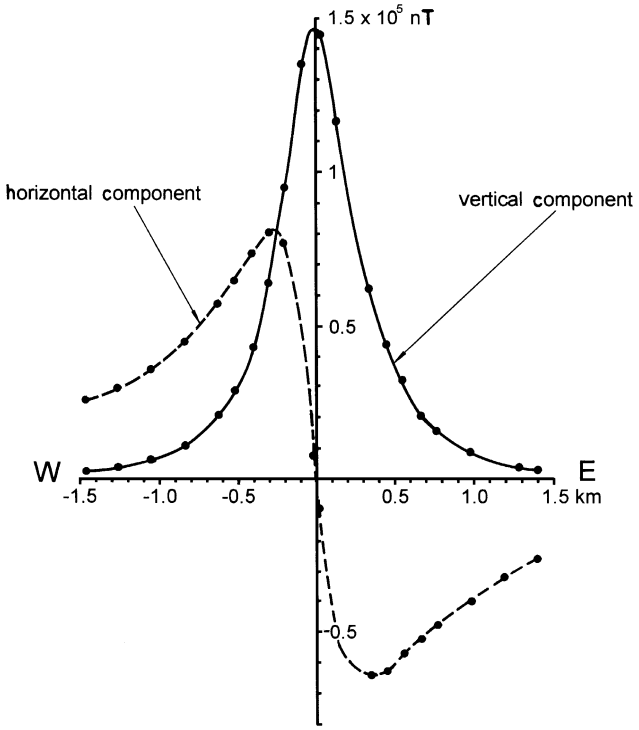

FIG. 10. Kursk anomaly. Vertical and horizontal components of the magnetic field over the orebody.

accordance with the known geology of the deposit. Although we do not have independent direct measurements of the depth to the source, our estimates are in agreement with results reported in the literature using Werner deconvolution.

For simplicity, we illustrated the proposed criteria with 2-D sources. The extension to 3-D sources may present computational but not theoretical difficulties.

ACKNOWLEDGMENTS

We thank Alan B. Reid, Harold Yarger, and an anonymous reviewer for valuable suggestions to improve the original version of this paper. J. B. C. S. and W. E. M. were supported in this research by fellowships from Conselho Nacional de Desenvolvimento Científico e Tecnológico (CNPq), Brazil.

REFERENCES

Barongo, J. O., 1984, Euler's differential equation and the identification of the magnetic point-pole and point-dipole sources: Geophysics, **49**, 1549–1553.

Beasley, C. W., and Golden, H. C., 1993, Application of Euler deconvolution to magnetic data from the Ashanti belt, southern Ghana: 63rd Ann. Internat. Mtg., Soc. Expl. Geophys., Expanded Abstracts, 417–420.

Bhattacharyya, B. K., 1967, Some general properties of potential fields in space and frequency domain: A review: Geoexploration, **5**, 127–143.

Davis, J. C., 1973, Statistics and data analysis in geology: John Wiley & Sons, Inc.

Emilia, D. A., 1973, Equivalent sources used as an analytic base for processing total magnetic field profiles: Geophysics, **38**, 339–348.

Fairhead, J. D., Bennett, K. J., Gordon, D. R. H., and Huang, D., 1994, Euler: Beyond the "black box": 64th Ann. Internat. Mtg., Soc. Expl. Geophys., Expanded Abstracts, 422–424.

Gunn, P. J., 1975, Linear transformations of gravity and magnetic fields: Geophys. Prosp., **23**, 300–312.

Hearst, R. B., and Morris, W. A., 1993, Interpretation of the Sudbury structure through Euler deconvolution: 63rd Ann. Internat. Mtg., Soc. Expl. Geophys., Expanded Abstracts, 421–424.

Hood, P., 1965, Gradient measurement in aeromagnetic surveying: Geophysics, **30**, 891–902.

Hsu, S., Sibuet, J., and Shyu, C., 1996, High-resolution detection of geologic boundaries from potential-field anomalies: An enhanced analytic signal technique: Geophysics, **61**, 373–386.

Loures, L. G. C. L., 1991, Interpretação aeromagnética automática com uso da equação homogênea de Euler e sua aplicação na Bacia do Solimões: M.Sc. thesis, Fed. Univ. of Pará, Brazil.

Paterson, N. R., Kwan, K. C. H., and Reford, S. W., 1991, Use of Euler deconvolution in recognizing magnetic anomalies of pipe-like bodies: 61st Ann. Internat. Mtg., Soc. Expl. Geophys., Expanded Abstracts, 642–645.

Ralston, A., and Rabinowitz, P., 1978, A first course in numerical analysis: McGraw-Hill Book Co. (Div. of McGraw-Hill, Inc.)

Reid, A. B., 1995, Euler deconvolution: Past, present and future—A review: 65th Ann. Internat. Mtg., Soc. Expl. Geophys., Expanded Abstracts, 272–273

Reid, A. B., Allsop, J. M., Granser, H., Millett, A. J., and Somerton, I. W., 1990, Magnetic interpretation in three dimensions using Euler deconvolution: Geophysics, **55**, 80–91.

Roest, W. R., and Pilkington, M., 1993, Identifying remanent magnetization effect in magnetic data: Geophysics, **58**, 653–659.

Ruddock, K. A., Slack, H. A., and Breiner, S., 1966, Method for determining depth and falloff rate of subteranean magnetic disturbances utilizing a plurarity of magnetometers: U.S. patent 3263161.

Slack, H. A., Lynch, V. M., and Langan, L., 1967, The geomagnetic gradiometer: Geophysics, **32**, 877–892.

Thompson, D. T., 1982, EULDPH: A new technique for making computer-assisted depth estimates from magnetic data: Geophysics: **47**, 31–37.

Werner, S., 1953, Interpretation of magnetic anomalies at sheet-like bodies: Sveriges Geol. Undersok., **C**, Arsbok **43** (1949), No. 6.

APPENDIX A
PROOF THAT $\langle \frac{\partial}{\partial \mathbf{x}}\mathbf{h}^o, \frac{\partial}{\partial \mathbf{z}}\mathbf{h}^o \rangle$ AND $\langle \mathbf{h}^o, \frac{\partial}{\partial \mathbf{x}}\mathbf{h}^o \rangle$, ARE NULL FOR LARGE INTERVALS

We first prove that $\langle (\partial/\partial x)\Delta T, (\partial/\partial z)\Delta T \rangle$ is null. The result holds for h^o because ΔT and h^o differ only by an additive constant.

Considering that ΔT is a harmonic function, we obtain from the solution of Laplace's equation in Cartesian coordinates with Dirichlet's boundary condition:

$$\Delta T(x,z) = \left[\sum_{n=1}^{\infty} A_n \sin(n\sqrt{\lambda x}) + B_n \cos(n\sqrt{\lambda}x)\right] \times [C\, e^{z\sqrt{\lambda}}], \quad \text{(A-1)}$$

where A_n, B_n, and C are constants and λ is a positive number. Differentiating equation (A-1) with respect to x we get

$$\frac{\partial \Delta T(x,z)}{\partial x} = \left[\sum_{n=1}^{\infty} n\sqrt{\lambda} A_n \cos(n\sqrt{\lambda}x) - n\sqrt{\lambda} B_n \sin(n\sqrt{\lambda}x)\right][Ce^{z\sqrt{\lambda}}]. \quad \text{(A-2)}$$

Differentiating with respect to z we obtain

$$\frac{\partial \Delta T(x,z)}{\partial z} = \left[\sum_{m=1}^{\infty} A_m \sin(m\sqrt{\lambda}x) + B_m \cos(m\sqrt{\lambda}x)\right][\sqrt{\lambda} C e^{z\sqrt{\lambda}}]. \quad \text{(A-3)}$$

The product of these two partial derivatives is

$$\begin{aligned}\frac{\partial \Delta T(x,z)}{\partial x}\frac{\partial \Delta T(x,z)}{\partial z} &= [\lambda C^2 e^{2z\sqrt{\lambda}}]\left[\sum_{m=1}^{\infty}\sum_{n=1}^{\infty} n A_n A_m \cos(n\sqrt{\lambda}x)\sin(m\sqrt{\lambda}x)\right. \\ &+ n A_n B_m \cos(n\sqrt{\lambda}x)\cos(m\sqrt{\lambda}x) \\ &- n B_n A_m \sin(n\sqrt{\lambda}x)\sin(m\sqrt{\lambda}x) \\ &\left. - n B_n B_m \sin(n\sqrt{\lambda}x)\cos(m\sqrt{\lambda}x)\right]. \quad \text{(A-4)}\end{aligned}$$

By integrating equation (A-4) with respect to x in interval $(-L, L)$ with L sufficiently large for this interval approximate the boundary $(-\infty, \infty)$, we obtain

$$\int_{-L}^{L} \frac{\partial \Delta T(x,z)}{\partial x} \frac{\partial \Delta T(x,z)}{\partial z}\, dx = [\lambda C^2 e^{2z\sqrt{\lambda}}] \left[\sum_{m=1}^{\infty} \sum_{n=1}^{\infty} n(A_n A_m - B_n B_m) \times \int_{-L}^{L} \cos(n\sqrt{\lambda}x) \sin(m\sqrt{\lambda}x)\, dx + n A_n B_m \int_{-L}^{L} \cos(n\sqrt{\lambda}x) \cos(m\sqrt{\lambda}x)\, dx - n B_n A_m \int_{-L}^{L} \sin(n\sqrt{\lambda}x) \sin(m\sqrt{\lambda}x)\, dx \right]. \quad \text{(A-5)}$$

Finally, using the orthogonality property of the trigonometric functions, we get

$$\int_{-L}^{L} \frac{\partial \Delta T(x,z)}{\partial x} \frac{\partial \Delta T(x,z)}{\partial z}\, dx = 0. \quad \text{(A-6)}$$

The inner product $\langle h^o, (\partial/\partial x) h^o \rangle$ is equal to $\langle \Delta T, (\partial/\partial x)\Delta T \rangle + b\langle \kappa, (\partial/\partial x)\Delta T \rangle$. The latter inner product is null because the integral of the total-field anomaly over the horizontal plane is zero (Bhattacharyya, 1967).

To prove that $\langle \Delta T(x), (\partial/\partial x)\Delta T(x) \rangle$ is also null, we follow the same reasoning above and note that multiplying equations (A-1) and (A-2) leads to the same products of trigonometric functions as before.